What Controls Photocatalytic Water Oxidation on Rutile TiO$_2$(110) under Ultra-High-Vacuum Conditions?

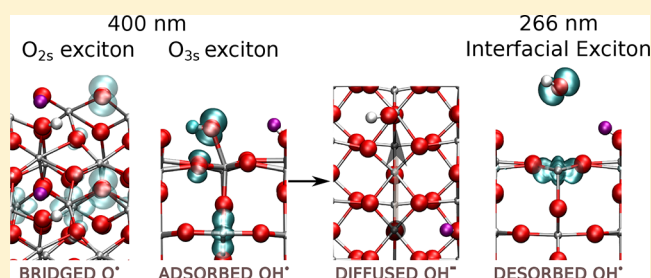Annapaola Migani*,[†],[‡] and Lluís Blancafort*,[§]

[†]Departament de Química Biològica i Modelització Molecular, IQAC-CSIC, Jordi Girona 18-26, 08034 Barcelona, Spain

[‡]Catalan Institute of Nanoscience and Nanotechnology (ICN2), CSIC and The Barcelona Institute of Science and Technology, Campus UAB, Bellaterra, 08193 Barcelona, Spain

[§]Institut de Química Computacional i Catàlisi and Departament de Química, Universitat de Girona (UDG), C/M. A. Capmany 69, 17003 Girona, Spain

Ⓢ Supporting Information

ABSTRACT: The photocatalytic O−H dissociation of water absorbed on a rutile TiO$_2$(110) surface in ultrahigh vacuum (UHV) is studied with spin-polarized density functional theory and a hybrid exchange-correlation functional (HSE06), treating the excited-state species as excitons with triplet multiplicity. This system is a model for the photocatalytic oxidation of water by TiO$_2$ in an aqueous medium, which is relevant for the oxygen evolution reaction and photo-degradation of organic pollutants. We provide a comprehensive mechanistic picture where the most representative paths correspond to excitonic configurations with the hole located on three- and two-coordinate surface oxygen atoms (O$_{3s}$ and O$_{2s}$). Our picture explains the formation of the species observed experimentally. At near band gap excitation, the O$_{3s}$ path leads to the generation of hydroxyl anions which diffuse on the surface, without net oxidation. In contrast, free hydroxyl radicals are formed at supra band gap excitation (e.g., 266 nm) from an interfacial exciton that undergoes O−H dissociation. The oxidation efficiency is low because the path associated with the O$_{2s}$ exciton, which is the most favored one thermodynamically, is unreactive because of a high propensity for charge recombination. Our results are also relevant to understand the reactivity in the liquid phase. We assign the photoluminescence measured for atomically flat TiO$_2$(110) surfaces in an aqueous medium to the O$_{3s}$ exciton, in line with the proposal based on experiments, and we have identified a species derived from the O$_{2s}$ exciton with an activated O$_{2s}$−Ti bond that may be relevant in photocatalytic applications in an aqueous medium.

400 nm
O$_{2s}$ exciton   O$_{3s}$ exciton

266 nm
Interfacial Exciton

BRIDGED O˙   ADSORBED OH˙   DIFFUSED OH⁻   DESORBED OH˙

1. INTRODUCTION

Photodriven heterogeneous catalysis has the potential to transform the way sustainable energy is generated.[1−3] It aims at an efficient conversion of the sun's energy into clean fuels by mimicking photosynthesis. One of the most prominent examples is the decomposition of water into molecular hydrogen and oxygen. Photoassisted electrolysis of water under irradiation with light and zero applied potential was demonstrated for the fist time in 1972 by Fujishima and Honda in an electrochemical cell using the TiO$_2$ semiconductor as the photoanode for the oxygen evolution reaction (OER).[4] Since this discovery, TiO$_2$ has become a benchmark material for understanding the OER in water splitting. Other important photocatalytic applications based on TiO$_2$ are photodegradation of organic pollutants in the gas and liquid phases or the development of materials with superhydrophilic or self-cleaning surface properties.[5]

In photodriven heterogeneous catalysis, the reactivity is promoted by the creation of a highly reactive intermediate through a photoredox reaction involving a hole−electron (h−e) pair. Some studies on TiO$_2$ point to free or adsorbed hydroxyl radicals generated from water molecules as the active

catalytic species.[6−8] However, the formation of adsorbed hydroxyl radicals from adsorbed water photooxidation by photogenerated valence band (VB) free holes has been questioned on the basis of the electron photoemission spectra of water adsorbed at the rutile TiO$_2$(110) surface under ultra-high-vacuum (UHV) conditions,[9−11] whose analysis indicates that the reaction is thermodynamically not possible because the water highest occupied orbital lies below the TiO$_2$ valence band maximum (VBM).[12] Alternatively, other studies assign the catalytically active species to O radical centers which originate from the trapping of the h at terminal 2-fold-coordinated substrate O atoms, O$_{2s}$ (bridging O atoms in TiO$_2$(110)).[12−19] One of the main questions in this discussion is whether the O of the active radical species is associated with an O atom from a water molecule or an O atom of the TiO$_2$ lattice.

Due to its implication in the photoelectrochemical water splitting on TiO$_2$, the photoinduced O−H bond dissociation of water adsorbed (H$_2$O$_{ads}$) on coordinately unsaturated Ti (Ti$_{cus}$) sites of single-crystal rutile TiO$_2$(110) (structure 1a, Figure 1)
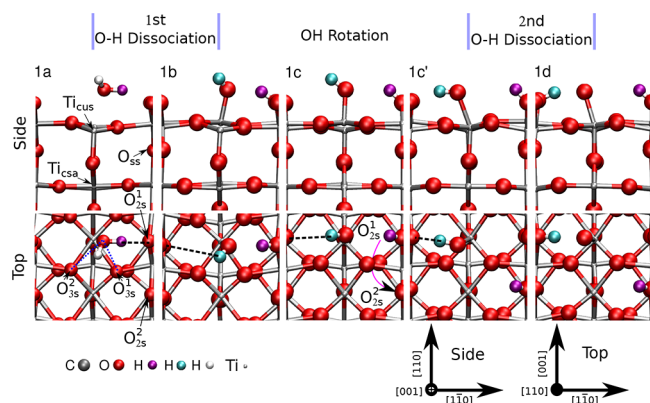
Figure 1. Schematics for the double, stepwise dissociation in the electronic ground state of 1/2 ML of H_2O adsorbed at a Ti_{cus} site of a $TiO_2(110)$-(1×2) supercell (side and top views). Structure 1a represents adsorbed water H_2O_{ads}, structures 1b, 1c, and 1c′ represent an adsorbed hydroxyl anion (OH_{ads}^-), and structure 1d represents an adsorbed oxyl dianion (O_{ads}^{2-}). The H atoms dissociated in the first and second steps are marked in magenta and cyan, respectively. The dashed lines in structures 1a, 1b, 1c, and 1c′ connect the surface 2-fold-coordinated bridging O, O_{2s}, and adsorbate H atoms involved in the interfacial H transfer. The magenta arrow in structure 1c (top view) indicates the displacement of the H dissociated in the first step from the O_{2s} adjacent to the occupied Ti_{cus} site, O_{2s}^1, to the O_{2s} adjacent to the empty Ti_{cus} site, O_{2s}^2 (see the Computational Details). The O_{2s}^1, O_{2s}^2, subsurface O (O_{ss}), 3-fold-coordinated surface O (O_{3s}^1, O_{3s}^2), coordinately saturated Ti (Ti_{csa}), and Ti_{cus} sites are labeled.

has been studied by surface science techniques in ultra-high-vacuum conditions.[20−22] This process is important as it represents the first and rate-determining step in the water oxidation (or OER) reaction.[23,24] Moreover, the intermediate radicals which are formed in the course of this reaction may play a crucial role in photodecomposition of harmful organic compounds. The electronic, structural, and chemical properties of a $TiO_2(110)$ surface under UHV conditions are largely different from those of TiO_2 in aqueous solutions.[13−16] For example, in an aqueous environment, water dissociation may involve proton transfer (PT) to a second water molecule.[25,26] Nevertheless, these detailed model studies also help to understand the mechanism of photoelectrochemical water splitting on TiO_2 electrodes and the formation of the active species in photocatalytic environmental remediation. They have established the currently accepted view of VB holes as the responsible species for water photodissociation.[20] In this paper, we study this model reaction computationally and we show how different types of hydroxyl radicals are generated and how they are related, thereby providing a global view of the primary events in the photogeneration of the key hydroxyl radical intermediates involved in photocatalysis.

Although the UHV experiments are conducted under well-defined conditions, the results point to a complex mechanism with several possible channels. The primary photochemical process is O−H bond dissociation where the water's H atom is transferred to the surface's 2-fold-coordinated bridging oxygen atom O_{2s} adjacent to the Ti_{cus} adsorption site, O_{2s}^1 (structure 1b, Figure 1).[20] The hydroxyl group that is formed at the Ti_{cus} site either diffuses to a Ti_{cus} site different from the original one[20] or desorbs.[20,22] Clear evidence that the ejected OH corresponds to radicals, i.e., $OH_{des}^\bullet$, was provided by time-of-flight (TOF) spectrometry,[22] whereas the electronic nature of the diffused hydroxyl group is undetermined.

Although H_2O_{ads} can be dissociated under UV irradiation, the dissociation efficiency is low. In ref 20, similar low dissociation probabilities are reported under irradiation with 400 nm (3.1 eV), 355 nm (3.49 eV), and 266 nm (4.66 eV) light at relatively high light intensity. The wavelength dependence was also examined by another group, which reported that water cannot be dissociated at 400 nm,[21] whereas at 266 nm[22] low dissociation probabilities similar to those of ref 20 are measured. Furthermore, dissociation of the second O−H bond to form an adsorbed oxyl dianion, O_{ads}^{2-} (structure 1d, Figure 1) or an adsorbed oxyl radical anion, $O_{ads}^{\bullet-}$, has not been observed.[20,22]

The mechanism of this important photoinduced catalytic process remains largely undetermined. However, the study on a fundamental level of the wavelength dependence of the photoredox reaction and the identification of the excitons and their reaction mechanisms is of utmost importance to understand the efficiency. Here, we employ 1/2 ML of H_2O adsorbed at a Ti_{cus} as a computational periodic model treated with spin-polarized density functional theory (DFT) with the HSE06[27] variant of the hybrid exchange-correlation functional HSE[28] to study the photoinduced catalytic dissociation of H_2O adsorbed at a Ti_{cus} as an excited-state process. With this approach, we can explicitly simulate the exciton, i.e., h−e pair, and the associated photochemical reaction coordinate. For a more comprehensive understanding of the deactivation after photoexcitation, we assess the competition between deactivation coordinates associated with different h−e pairs.

The mechanistic picture arising from our results is summarized in Figure 2. For our system, the H_2O_{ads} highest occupied levels lie below the VBM.[29] Laser excitation may give rise to different excitons depending on the energy. Excitation energies near the band gap (400 nm) generate a bulk exciton which can relax to different minima where the h is localized on different sites. There are two important minima where the h is localized on the 3-fold-coordinated surface O atom interacting with the adsorbed water, O_{3s}^1, and the 2-fold-coordinated bridging O atom adjacent to the empty Ti_{cus} site, O_{2s}^2 (Figure 1). The O_{3s}^1 localized exciton triggers the O−H dissociation of the adsorbed water through an interfacial proton-coupled electron transfer (PCET) mechanism[30] and yields an excited-state adsorbed hydroxyl radical transient species which is hemibonded to the surface, $OH_{hmb}^\bullet$. After 400 nm excitation, this species can undergo h−e recombination, leading to adsorbed hydroxyl anions on the ground state, which can diffuse on the surface, OH_{dif}^-. The second dissociation step to yield $O_{ads}^{\bullet-}$ is thermodynamically unlikely. In turn, the O_{2s}^2 localized exciton follows nonradiative charge carrier separation followed by a proton transfer, which leads to a ground-state transient with a hydroxyl anion adsorbed at the Ti_{cus} site and a protonated neighboring bridging atom, $O_{2s}^1H^-$. The bulk exciton can also relax to other excitons which will ultimately undergo nonradiative h−e recombination to yield intact water. In contrast, high excitation energies (266 nm) can lead to an interfacial exciton where the e is excited from an occupied valence band level partly localized on the $TiO_2(110)$ surface and H_2O_{ads} orbitals. This initiates the oxidation of the adsorbate, which is followed by H transfer to the surface and leads to $OH_{ads}^\bullet$. At this excitation energy, $OH_{ads}^\bullet$ can desorb from the surface, generating free $OH_{des}^\bullet$ radicals.

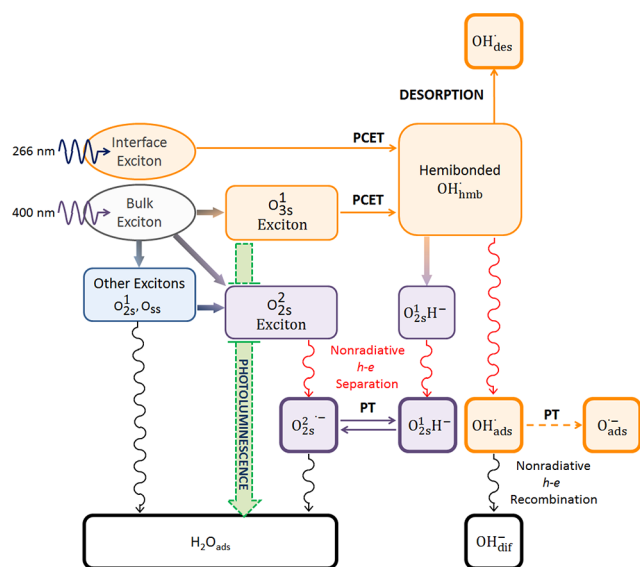**Figure 2.** Global scheme for photocatalytic H_2O_{ads} oxidation under UHV conditions showing the formation of different radical intermediates depending on the excitation wavelength. The color code indicates species associated with (orange) O_{3s}^2, (purple) O_{2s}^2, and (blue) other excitons. Excited- and ground-state species are in plain and bold frames. Wiggly arrows indicate (red) nonradiative h−e separation between excited- and ground-state species and (black) h−e recombination between ground-state open- and closed-shell configurations. Dashed arrows indicate unlikely processes. Free hydroxyl radicals $OH_{des}^•$ are formed with supra band gap excitation (266 nm) through an interfacial exciton where the photogenerated h is partly on the adsorbed water. The $OH_{ads}^•$ and $(O_{2s}^2)^{•−}$ radicals can be formed with band gap excitations from the O_{3s}^1 and O_{2s}^2 excitons, respectively. The oxidation of adsorbed water by the O_{3s}^1 excitons occurs via interfacial PCET. These radical intermediates are transient species prone to undergo nonradiative h−e pair recombination, leading to the unoxidized diffused hydroxyl anion, $OH_{dif}^−$, and intact adsorbed water, H_2O_{ads}, respectively.

2. COMPUTATIONAL DETAILS

We use a periodic model where the unit cells contain a $TiO_2(110)$ slab made of five three-atom-thick layers, employ the experimental lattice parameters for bulk rutile TiO_2 (a = 4.5941 Å, c = 2.958 Å),[31] and include at least 10 Å of vacuum between repeated images. We use a pristine surface model because the concentration of oxygen vacancies in the UHV experiments of ref 20 is only 0.08 ML and the majority of molecules (91%) are adsorbed at Ti_{cus} sites, away from the vacancies. See the Supporting Information for a discussion on the suitability of the model for excited-state calculations.

We model a 1/2 ML coverage, repeating the $TiO_2(110)$-(1 × 1) unit cell along the [001] direction. This coverage is higher than that of 0.02−0.05 ML used in the UHV experiments.[20] Modeling lower coverages would require larger supercells, which is not affordable with our computational setup, but we expect that the coverage effect on the energy profiles will be small because the neighboring water molecules do not participate directly in the reaction of the dissociating one. However, our coverage does affect the second O−H bond dissociation step. For this step we consider as the acceptor site the O_{2s} nearest neighbor to the dissociating H atom (dashed arrow in the top view of structures 1b, 1c, and 1c′, Figure 1). In our $TiO_2(110)$-(1 × 2) supercell, this atom is equivalent to the O_{2s} site involved in the first O−H bond dissociation, O_{2s}^1. As a result, transfer of both H atoms to this site is not possible. Therefore, after the O−H dissociation step, we move the dissociated H atom to the O_{2s} atom adjacent to the empty Ti_{cus} site, O_{2s}^2 (cf. structures 1c and 1c′, Figure 1) to allow for the second interfacial H transfer. This has a negligible effect on the energies (see below and Figure S1, Supporting Information). Finally,

to model the second O−H bond dissociation for the exciton with the h localized at the O_{2s}^2 site, we need three O_{2s} sites, the first one for the h, the second one for the first dissociated H, and the third one for the second dissociated H. In this case, we employ a 1 × 3 supercell, which is triplicated in the [001] direction.

All calculations are performed using VASP within the projector augmented wave (PAW) scheme.[32] We employ a plane-wave energy cutoff of 445 eV, an electronic temperature $k_BT \approx 0.2$ eV with all energies extrapolated to $T \to 0$ K, and a PAW pseudopotential for Ti which includes the $3s^2$ and $3p^6$ semicore levels. The calculations use the HSE06 functional.[27,28] HSE06 gives accurate electronic and optical band gaps for anatase and rutile bulk TiO_2[33−35] and the cathecol on the $TiO_2(110)$ interface.[36−38] Moreover, it gives accurate absolute alignments of the valence band maximum (VBM) and conduction band minimum (CBM) for the plain $TiO_2(110)$ surface[33] and interfacial alignments of the adsorbate levels for water and methanol on $TiO_2(110)$ interfaces.[29,34,35] All computationally intensive HSE06 ground- and excited-state optimizations have been performed employing the Γ-point only. Since the slabs exhibit nonzero dipole moments along the [110] direction, dipole corrections have been applied to the potential, total energies, and forces. The geometries are fully relaxed with all forces $\lesssim$0.02 eV/Å.

The DFT HSE06 calculations to model the closed-shell ground-state configurations are performed spin unpolarized. Following our previous work,[30] the exciton states are computed as open-shell configurations with two unpaired electrons occupying 2p and 3d orbitals of specific O and Ti sites by means of spin-polarized DFT HSE06 calculations with triplet spin multiplicity. Spin-polarized DFT HSE06 gives a localized description of the h−e pair. h and e localization is accompanied by a polaronic distortion of the lattice at the corresponding O and Ti sites. Accordingly, to converge a given h−e configuration, a small lattice distortion is applied at the relevant O and Ti sites of the input structure of the geometry optimization. This procedure drives the geometry optimization toward the convergence of a minimum energy structure with the desired electronic configuration. We use the climbing-image nudged elastic band (CI-NEB)[39] method to compute the reaction coordinates and barriers with four intermediate images. The starting geometries of the images are obtained by interpolating the geometries of the reactant and product minima with their centers of mass aligned employing the "aconvasp" utility of the aflow program.[40]

Our triplet calculations are an approximation to more expensive structure optimizations on S_1 computing the h−e pair as an excited state with singlet spin multiplicity. This could be done using, for example, the Bethe Salpeter equation (BSE) method,[41,42] but it is not feasible for our system. The difference between the singlet and triplet energies is primarily due to the exchange integral between the h and e orbitals, which can be expected to be small because the h and the e are located on different sites and have small overlap. Therefore, we expect the energy difference between T_1 and S_1 excited states with similar electronic nature to be within a few tenths of an electronvolt, so that the mechanistic picture will not change. To confirm the reliability of this approach, we compute the S_1 excited state with the BSE method (see the Supporting Information for details) for the ground-state reactant minimum, i.e., Franck−Condon (FC) geometry, and compare it with T_1 from the DFT calculation. The S_1 and T_1 energies are ∼3.55 and ∼3.22 eV, respectively, which is consistent with our theoretical argument. This difference is also in agreement with previous estimates of the singlet−triplet gap in a minimal $Ti(OH)_4$ model of ∼0.1−0.3 eV.[43] The density of states (DOS) from the underlying DFT HSE06 calculation and the singlet excitation energies from the BSE calculation are used in Figures 4 and 7, respectively. In Figure 7, the excitations (indigo lines) have been shifted by 0.33 eV so that S_1 matches the T_1 vertical excitation.

To provide further support for the importance of excitons, we have calculated the exciton binding energy E_b of S_1 at the FC point and an excited-state minimum (O_{3s}^1; see below) according to

$$E_b = (\varepsilon_{CBM} - \varepsilon_{VBM}) - E_1 \qquad (1)$$

where E_1 is the S_1 energy and ε_{CBM} and ε_{VBM} are the CBM and VBM Kohn–Sham (KS) energies, respectively. For the FC point, the lowest energy exciton binding energy is ~0.08 eV, which is of the same order of magnitude as that computed for bulk rutile TiO_2, with similar computational approaches.[34,44] For the excited-state minimum, E_b increases to ~0.31 eV. This increase shows the importance of describing the reactivity in terms of an excited state corresponding to a h–e pair configuration, as it indicates that exciton surface localization may compete with formation of uncorrelated h–e pairs. In this context, a bound exciton resonance with a near-band energy gap (3.76 eV) has been recently characterized for bulk anatase.[45]

The adsorption energy E_{ads} is given by

$$E_{ads} \approx E[\text{water} + TiO_2(110)] - E[TiO_2(110)] - E[\text{water}] \tag{2}$$

where $E[\text{water} + TiO_2(110)]$, $E[TiO_2(110)]$, and $E[\text{water}]$ are the total energies of the covered and clean surfaces and gas-phase water molecule, respectively. The computed adsorption energy for 1/2 ML of intact and dissociated water adsorbed at a Ti_{cus} site, namely, structures 1a and 1b in Figure 1, are ~−1.05 and ~−1.10 eV, respectively. These values are in very good agreement with previously reported values with DFT HSE06.[46]

3. RESULTS

3.1. Reactant Minima and h–e Configurations. We take a perspective similar to that adopted in computational photochemistry[47−50] and describe the oxidation as an excited-state process carried out by a specific exciton (Figure 2). This implies that we do not assume charge carrier separation and include the synergic role of holes and electrons in the heterogeneous photocatalytic oxidation process. This is a proper perspective given that the UV irradiation experiments are conducted in absence of an applied external potential, which would prompt an early h–e pair separation. Supra band gap irradiation by UV light induces a VB to CB electronic transition and thus results in the creation of h–e pairs where the h and e are delocalized. The photogenerated excitons become trapped, i.e., localized, on or near the surface upon nuclear relaxation following photoexcitation. The nuclear relaxation and trapping of photogenerated exciton pairs has been investigated for the anatase TiO_2 bulk, (101) surface, and nanoparticles, but the photochemical reactivity was not considered in these works.[51,52] Here we discuss a similar process for rutile $TiO_2(110)$ and focus on the reactivity of the relaxed h–e pairs.

The most important configurations for catalysis are those that have the h localized at surface sites because they can react with the adsorbate. In $TiO_2(110)$, there are two possible surface sites for h localization, the O_{3s} and the O_{2s} atoms (Figure 1). We know from our work on the photooxidation of CH_3OH adsorbed at a Ti_{cus} site of $TiO_2(110)$ that the important site for oxidation is the O_{3s} atom with the shortest distance to the adsorbate O atom, O_{3s}^1 in Figure 1.[30] In addition, the thermodynamically most stable sites for h localization are the O_{2s} atoms because of their lower coordination number.[30,53−55] In our model for 1/2 ML of H_2O_{ads} at a Ti_{cus} site, there are two nonequivalent O_{2s} atoms adjacent to the occupied and empty Ti_{cus} sites, O_{2s}^1 and O_{2s}^2, respectively, in Figure 1. These sites are not active in the oxidation of H_2O_{ads} at a Ti_{cus} site, which is in contrast to their active role in the oxidation of H_2O not adsorbed at TiO_2/aqueous interfaces.[14−16,56,57] However, in our system under UHV conditions, they account for benign reaction paths, which are in competition with H_2O_{ads} oxidation by the O_{3s}^1 site. We center the discussion of the competing paths on the O_{2s}^2 site, which is the best electron donor because it does not form a H

bond with H_2O_{ads} and therefore gives the most stable h–e configurations. This species is representative of other configurations that we have located with the h localized at the O_{2s}^1 site and a subsurface O (O_{ss}) site (see Figure S2 in the Supporting Information), which we expect to decay to the thermodynamically more favorable configuration or follow a similar fate.

For the O_{2s}^2 site, we could optimize the minima for the electronic configurations with the e at the Ti_{cus} and Ti_{csa} sites (structures 3a and 3b, respectively, Figure 3), with energies of
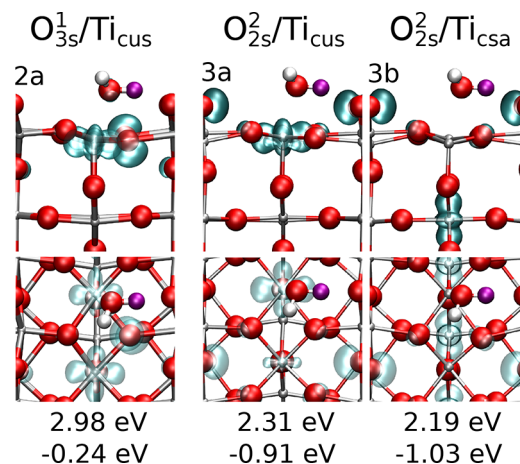

O_{3s}^1/Ti_{cus}	O_{2s}^2/Ti_{cus}	O_{2s}^2/Ti_{csa}
2a	3a	3b
2.98 eV	2.31 eV	2.19 eV
-0.24 eV	-0.91 eV	-1.03 eV

Figure 3. Spin density at reactant minima of surface-localized excitons with (structure 2a) O_{3s}^1/Ti_{cus}, (structure 3a) O_{2s}^2/Ti_{cus}, and (structure 3b) O_{2s}^2/Ti_{csa} configurations: (top values) minimum energies relative to the energy of the ground-state reactant minimum 1a and (bottom values) exciton relaxation energy relative to the vertical excitation energy of ~3.22 eV. Structure 3b is the thermodynamically most stable exciton, and structure 2a is the one giving the oxidation process.

~2.31 and ~2.19 eV relative to the ground-state minimum 1a. The most stable minimum by ~0.12 eV has the largest charge carrier separation with the e at the Ti_{csa} site, structure 3b, which indicates a weak interaction between the h and the e.

In contrast, for the O_{3s}^1 site, we could only optimize the minimum of the electronic configuration with the e located at the Ti_{cus} site (structure 2a, Figure 3), with a relative energy of ~2.98 eV. In this arrangement, the h and e are located very close to each other and are strongly interacting. This result indicates that h localization at the O_{3s}^1 site is only possible upon concomitant e localization at the surface Ti_{cus} site. It also explains why the role of O_{3s}^1 has been overlooked in previous theoretical studies on rutile $TiO_2(110)$, which do not include the excited e and assume that the oxidation is carried out by an independent h.[53,55,56,58,59] One of these studies reports localization of a h at an O_{3s} site of a plain surface with an essentially null trapping energy, indicating the absence of propensity to trap the h at O_{3s}.[53] Instead, we find that the concomitant localization of the e at the Ti_{cus} site and the incipient interaction of the h at the O_{3s}^1 site with the water O atom, i.e., incipient $O_{3s}^1–O_{ads}$ hemibond formation, results in a minimum which is stabilized by ~0.24 eV with respect to the vertical excitation energy of ~3.22 eV.

The O_{3s}^1/Ti_{cus} minimum 2a is ~0.79 eV higher than the O_{2s}^2/Ti_{csa} minimum 3b. This trend is in agreement with previous theoretical studies which compared relative h stabilities at O_{2s} sites not involved in H-bond interactions and O_{3s} sites.[53,54] However, an excited-state reaction is not an equilibrated

process and does not necessarily imply relaxation to the most stable excited-state minimum of the reactant. Reactivity can also arise from an excited-state minimum that is energetically accessible relative to the vertical excitation energy, although it is not the lowest energy excited-state minimum. This is precisely the case for the photoinduced oxidation of H_2O_{ads} at Ti_{cus}, which is linked to the interaction with the O_{3s} site.

The formation of the excited-state minimum 2a upon excitation of structure 1a with band gap energy can be understood as the result of a polarization of the VBM during the nuclear relaxation, as illustrated in Figure 4. The VBM of
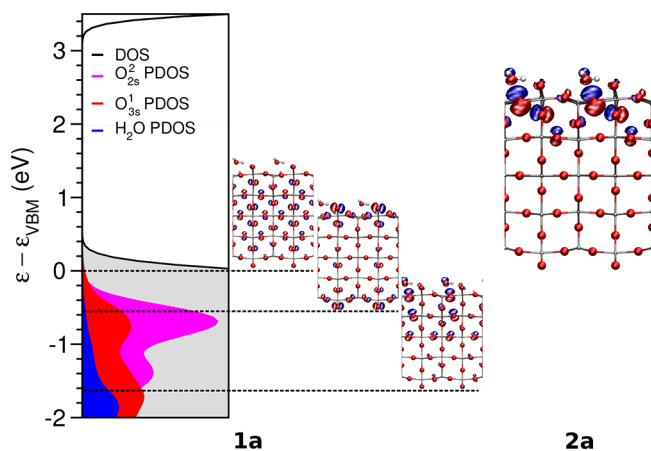

Figure 4. (Left) Total (black) density of states (DOS) and H_2O (blue), O_{2s}^2 (magenta), and O_{3s}^1 (red) projected density of states (PDOS) for the ground-state reactant minimum 1a. Energies are relative to the valence band maximum, ε_{VBM}. Filling denotes occupation. Horizontal dashed lines denote the VBM and selected orbital energies and orbitals. (Right) VBM orbital for O_{3s}^1/Ti_{cus} excited-state reactant minimum 2a. The 1×2 unit cell is duplicated along the $[1\bar{1}0]$ direction in the orbital representation. The DOS, PDOS, and VBM orbitals are from the $4 \times 4 \times 1$ k-point mesh DFT HSE06 calculations described in the Supporting Information.

structure 1a is the totally antibonding combination of O $2p_\pi$ atomic orbitals along the $[110]$ and $[1\bar{1}0]$ directions[35,60] (see Figure 4, left). It is delocalized across 3-fold-coordinated O_{ss} and interior O (O_{in}) sites, with a small weight on the surface O_{3s} atoms, and it has a shape similar to that of the orbitals involved in the S_1 excitation of TiO_2 rutile nanoparticles.[61] Upon relaxation to structure 2a, the VBM is polarized toward the O_{3s}^1 and O_{ss} atoms (see Figure 4, right). There is also a reordering of the H_2O_{ads} levels, so that the H_2O_{ads} highest occupied molecular orbital ($1b_1$) also contributes to the VBM. This provides structure 2a with a small interfacial charge-transfer character, while it can be predominantly described as a surface exciton (see the spin density in Figure 3).

The interfacial level alignment of the water $1b_1$ orbital relative to the VBM (Figure 4, left) is in agreement with accurate many-body quasiparticle calculations and the UPS spectra of H_2O_{ads} on $TiO_2(110)$ under UHV conditions.[9−11] The calculations support the conclusion that photooxidation of H_2O_{ads} at a Ti_{cus} site of $TiO_2(110)$ by a photogenerated VB free h is thermodynamically not possible because the water $1b_1$ orbital lies below the TiO_2 VBM.[12] In contrast, the h transfer from the TiO_2 substrate to H_2O_{ads} is thermodynamically possible at the 2a minimum, where the O_{3s}^1 $2p_\pi$ and H_2O_{ads} $1b_1$ orbitals that interchange the h are both major contributors to the $TiO_2(110)$ VBM (Figure 4, right) as a consequence of

coupled nuclear and electronic relaxation. This indicates that oxidation of H_2O_{ads} under UHV conditions occurs via an indirect mechanism involving a surface localized rather than a free VB h.

The first insight into the wavelength dependence can be obtained by examining the projected density of states (PDOS) at minimum 1a. The highest energy levels with contributions from the O_{2s}^2 and O_{3s}^1 sites are located ~−0.55 and ~−1.63 eV below the VBM. Accordingly, surface excitons with O_{2s}^2 character and interfacial excitons with O_{3s}^1 character can be directly photogenerated with supra band gap excitations. In particular, photogeneration of the interfacial excitons with O_{3s}^1 character requires excitation energies that exceed by ~−1.6 eV the band gap excitation energy, which is consistent with the 266 nm light used in some experiments.[22]

In the following, we will focus on the reactivity of the most stable O_{2s}^2/Ti_{csa} and higher lying O_{3s}^1/Ti_{cus} excitons. The competition between these reaction channels explains the experimental behavior.

3.2. Reactivity of the O_{3s}^1 Exciton. The reactivity of the O_{3s}^1 exciton is shown in Figure 5. At the O_{3s}^1/Ti_{cus} minimum 2a, the energy separation between the excited and ground states is ~1.75 eV (Figure 5). This suggests that an analogous species is responsible for the photoluminescence bands peaking at 810 nm (1.53 eV) and 840 nm (1.48 eV) observed for the rutile $TiO_2(110)$ and $TiO_2(001)$ surfaces in solution, respectively. These bands have been assigned to a surface-trapped hole (STH) formed at triply coordinated O_{3s},[14−16] without specifying the position of the electron, and we suggest that the species undergoing radiative charge carrier recombination may be an exciton localized on the surface.

The O_{3s}^1/Ti_{cus} exciton can evolve after O−H bond dissociation to adsorbed $OH_{ads}^\bullet$ and $O_{ads}^{\bullet-}$ species or to the desorbed $OH_{des}^\bullet$ radical. The two paths are shown in parts a and b, respectively, of Figure 5. The first step common to both reaction paths corresponds to the first O−H bond dissociation, which takes place via PCET.[25,57,58,62−66] This is similar to what we recently reported for the O−H bond dissociation of CH_3OH on $TiO_2(110)$.[30] In this mechanism, the h is transferred from the substrate O_{3s}^1 site to the adsorbate O atom, O_{ads}, and simultaneously, a proton is transferred from the adsorbate to the substrate O_{2s}^1 site adjacent to the occupied Ti_{cus} site.[30] In contrast to CH_3OH, for H_2O, we find that the h is only partially transferred to the adsorbate (cf. spin densities of O_{3s}^1/Ti_{cus} and $O_{3s}^1-O_{ads}/Ti_{cus}$ in Figure 5a). This leads to the product minimum 2b with the e at the Ti_{cus} site and the h shared between the O_{3s}^1 and O_{ads} sites, which corresponds to a three-electron, two-atom hemibond.[54,67,68] Structure 2b corresponds to an excited-state hemibonded hydroxyl radical, $OH_{hmb}^\bullet$. Despite an extensive search, we have not found a minimum where the h is fully localized on the OH adsorbate. In the hemibonded configuration, the OH_{ads} charge decreases by ~0.54 electron relative to that of the ground-state minimum 1a. The path is exothermic by ~0.27 eV and is essentially barrierless. This is in contrast to the O−H dissociation of the configurations with the h localized at the O_{2s}^1 and O_{ss} sites (Figure S2, Supporting Information) and the O_{2s}^2 site (Figure 6), which have activation barriers of ~0.2−0.3 eV and are endothermic by ~0.1−0.3 eV. This shows that the simultaneous partial electron transfer stabilizes the proton-transfer product and lowers the barrier. The low barrier also implies that structure 2a will be hardly luminescent under UHV conditions (dashed green arrow in Figure 2).
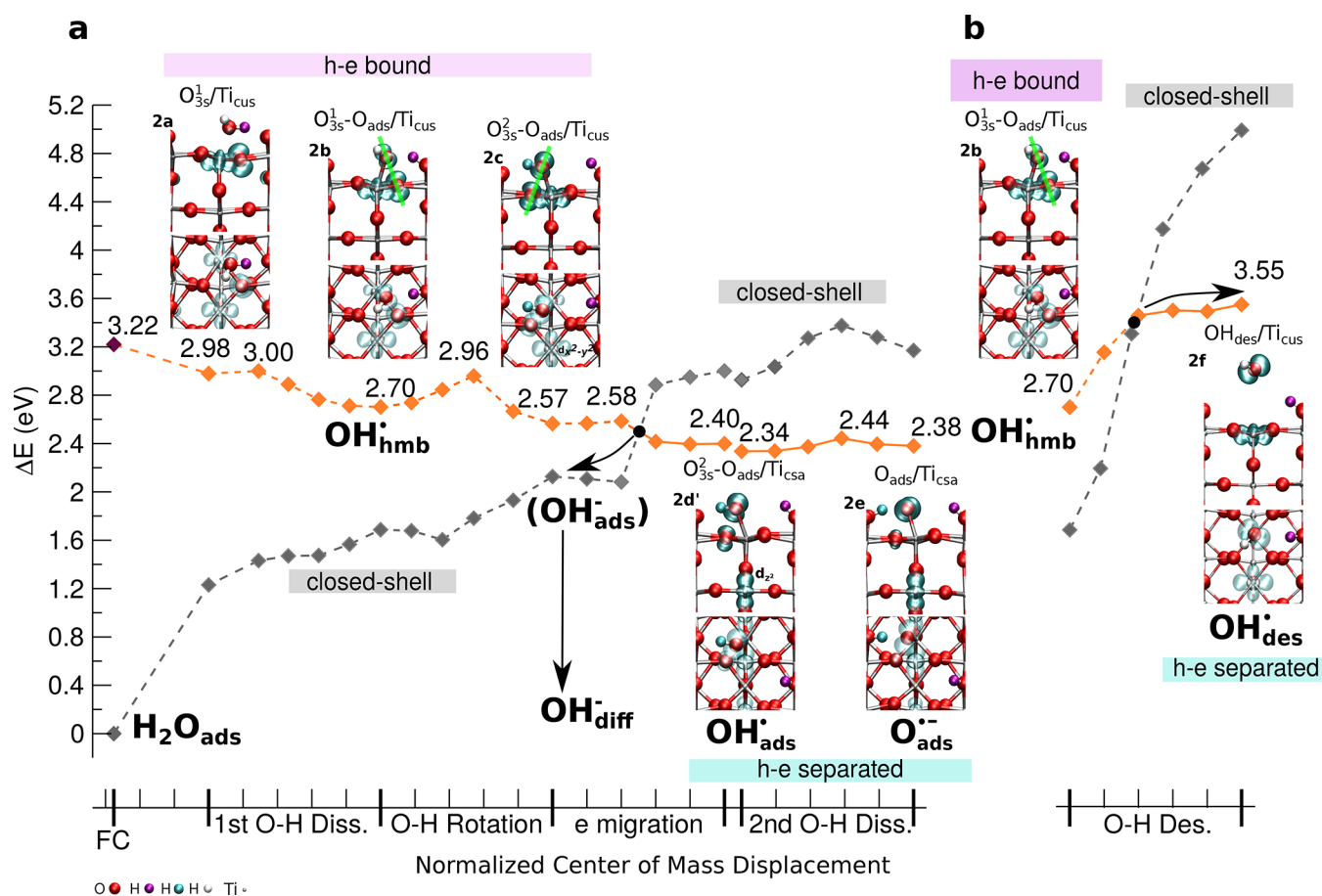
Figure 5. Energy profile of the ground and excited states along the multistep H_2O_{ads} oxidation coordinates associated with the O^1_{3s} exciton. The different steps are described on the x-axes. Panel a shows the transformation of the O^1_{3s} excited-state reactant minimum (2a) to the $O_{ads}^{\bullet-}$ product (2e) through intermediates 2b, 2c, and 2d′. Panel b shows the alternative path from the 2b minimum to give the $OH_{des}^{\bullet}$ product. Dashed and solid orange lines denote bound and separated h−e pairs, respectively, and dashed gray lines a closed-shell configuration. Spin densities, structures, and electronic-configuration labels are shown for the minima. The arrows from the crossings highlight the paths that lead to the experimentally observed products.

At the hemibonded product minimum 2b, both the O^1_{3s}−O_{ads} and the O_{ads}−Ti_{cus} distances are shorter with respect to those of the reactant minimum 2a (∼2.24 Å versus ∼2.57 Å and ∼1.98 Å versus ∼2.14 Å, respectively). This indicates a strong interaction between the excitonic h−e pair and the OH adsorbate. Accordingly, charge carrier separation via e migration from the bare Ti_{cus} site to the Ti_{csa} site is endothermic by ∼0.1 eV (Figure S2, Supporting Information).

From the 2b minimum, the path to the $OH_{ads}^{\bullet}$ and $O_{ads}^{\bullet-}$ products (Figure 5a) proceeds through a second interfacial H transfer to the nearest O^1_{2s} site, backward with respect to the direction of the first O−H dissociation. This is preceded by the formation of the corresponding interfacial H bond, which is achieved by a clockwise rotation of the OH adsorbate around the O_{ads}−Ti_{cus} axis. This rotation reduces the interfacial distance between the adsorbate H and O^1_{2s} atoms involved in the second O−H bond dissociation event from ∼3.63 to ∼1.78 Å. There is a sizable barrier of ∼0.26 eV due to the breaking of the O^1_{3s}−O_{ads} hemibond. However, the process is exothermic by ∼0.13 eV because a new hemibond between the adsorbate O and the surface O^2_{3s} atom is formed (cf. structures 2b and 2c).

Upon dissociation, the surface-localized e becomes polarized at the farthest Ti_{cus} site from the protonated O^1_{2s} atom, i.e., bare Ti_{cus}. The polarization is driven by electrostatic effects because the negative charge of the O^1_{2s}H group is ∼0.56 electron larger

than that of the bare O^2_{2s} atom. Thus, the polarization minimizes the electrostatic repulsion with the excitonic e. This difference is due to the charge transfer of ∼0.44 electron accompanying the proton transfer (see Table S2, Supporting Information).

As a result of the rotation, the OH_{ads} charge further decreases by ∼0.15 electron, indicating that the O^2_{3s}−O_{ads} hemibond becomes additionally localized toward OH_{ads} in structure 2c. This is possible because the donating capability of the OH_{ads} is increased once the interfacial H bond with the O^1_{2s}H group is broken. This polarization of the hemibond decreases the charge carrier interaction. As a result, we find that the h−e separation via e migration to the Ti_{csa} underneath the surface becomes thermodynamically favored from the O^2_{3s}−O_{ads} hemibonded minimum 2c. This leads to a charge-separated minimum 2d with an adsorbed hydroxyl radical $OH_{ads}^{\bullet}$ hemibonded to the $TiO_2(110)$ substrate, located at ∼2.40 eV.

The charge separation takes place together with the decay of the exciton to the ground state through a state crossing. After the crossing, the configuration of the states is inverted; i.e., the open-shell (orange line) and closed-shell (gray line) configurations become the ground and excited states, respectively. Before the crossing, the open-shell configuration is given by a bound h−e pair (dashed orange line), while, after the crossing,
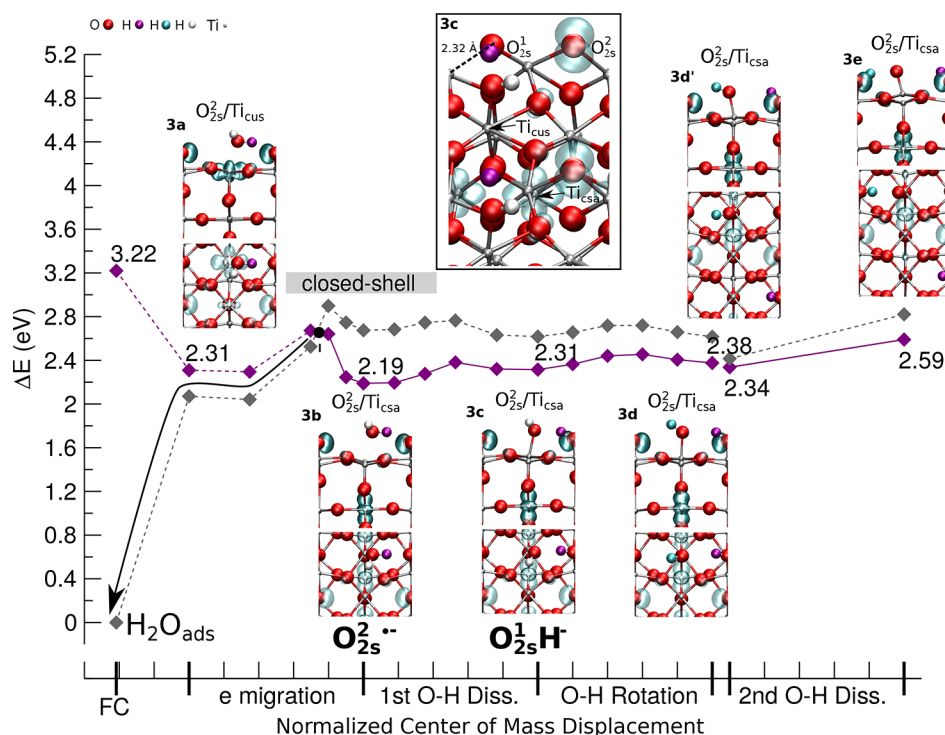
Figure 6. Energy profile of the ground and excited states along the multistep H_2O_{ads} dissociation coordinate associated with the O_{2s}^2 exciton. The different steps are shown on the x-axis. The dashed and solid purple lines indicate the open-shell O_{2s}^2/Ti_{cus} and O_{2s}^2/Ti_{csa} configurations, respectively, and the dashed gray line indicates the closed-shell configuration. Spin densities, structures, and electronic-configuration labels are shown for the minima. The inset shows the activation of one of the O−Ti bonds at minimum 3c. The arrow from the crossing highlights the most probable relaxation path based on the slopes of the intersecting states. The reaction coordinates are given in normalized center of mass displacement.

the open-shell configuration is given by a charge-separated h−e pair (solid orange line).

The charge separation is accompanied by a further polarization of the hemibond and a decrease of the OH_{ads} charge by ∼0.13 electron. This prompts the second O−H bond dissociation, which takes place on the ground state and involves a slightly activated (∼0.10 eV) and endothermic reaction coordinate from the 2d′ minimum. The H dissociation corresponds to a PT, which further increases the adsorbate negative charge by ∼0.48 electron and yields an adsorbed oxyl radical anion ($O_{ads}^{•−}$), corresponding to the minimum 2e at ∼2.38 eV. This in turn strengthens the O_{ads}−Ti_{cus} bond, resulting in a shorter bond (∼1.93 Å). At the same time, the hemibond becomes further polarized toward the adsorbate, and the O_{ads}−O_{3s}^2 distance increases to ∼2.50 Å. Complete h localization on the O_{ads} atom has a small energetic cost of ∼0.2 eV.

An analogous path for the $OH_{ads}^{•}$ to $O_{ads}^{•−}$ step has been reported for the liquid H_2O/$TiO_2(110)$ interface.[67] The oxyl radical anion $O_{ads}^{•−}$ has also been detected spectroscopically as a transient for the related n-SrTiO$_3$/aqueous interface by means of a vibrational signature involving a subsurface Ti−O vibration in the plane right below the adsorption site.[69,70] In our case, along the reaction path from structure 2b to structure 2e, we observe significant changes of the Ti_{cus}−O_{ss} length (see Table S1, Supporting Information) which are consistent with the activation of this vibration.

At the crossing, an alternative path to the second O−H bond dissociation is nonradiative charge carrier recombination leading to an unoxidized product with closed-shell configuration, the $OH_{ads}^{−}$ species. A quantitative determination of the branching at the crossing can only be made with nonadiabatic

dynamics, but the rather flat energy profile along the O−H dissociation suggests that charge recombination will be the preferred process. The high-energy $OH_{ads}^{−}$ species can relax to the ground-state $OH_{ads}^{−}$ minimum. The ∼2.5 eV excess energy released in the nonradiative decay is redistributed to internal vibrational modes (i.e., internal vibrational redistribution, IVR), especially those that are directly coupled to the electronic excitation, such as the interfacial O_{ads}−Ti_{cus} distance, and this suggests that the decay will be followed by diffusion, leading to diffused hydroxyl anions, $OH_{dif}^{−}$. For comparison, the energy barrier for diffusion of water monomers on $TiO_2(110)$ is only ∼0.5 eV,[71] which suggests that the released energy will be sufficient to induce diffusion of $OH_{ads}^{−}$. In fact, the species detected experimentally after UV irradiation is diffused $OH_{dif}^{−}$ and not $OH_{ads}^{•}$ or $O_{ads}^{•−}$.[20−22] Overall, this indicates that the second O−H dissociation is prevented by the low exothermicity and the competing charge recombination at the crossing, which ultimately may lead to hydroxyl anion diffusion.

The excited H_2O_{ads} to $OH_{ads}^{•}$/$O_{ads}^{•−}$ path is exothermic by ∼0.8 eV. The equivalent path for the photoinduced oxidation of CH_3OH_{ads} at a Ti_{cus} site to $CH_2O_{ads}^{•−}$ is exothermic by ∼1.9 eV.[30] This difference explains why the $CH_2O_{ads}^{•−}$ is a stable detectable species,[21,72−77] whereas the $OH_{ads}^{•}$/$O_{ads}^{•−}$ products located at ∼2.38 eV/∼2.40 eV are transient species which may only be detected with time-resolved spectroscopy techniques.

In contrast to the $OH_{ads}^{•}$ and $O_{ads}^{•−}$ species,[20,22] the $OH_{des}^{•}$ product has been detected experimentally.[22] Figure 5b shows the $OH_{des}^{•}$ formation mechanism from structure 2b. This mechanism is also mediated by a state crossing, consistently with other photodesorption processes on $TiO_2(110)$.[78] Along this path, structure 2b may lead to structure 2f (see the arrow indicating the product formation), which has the same
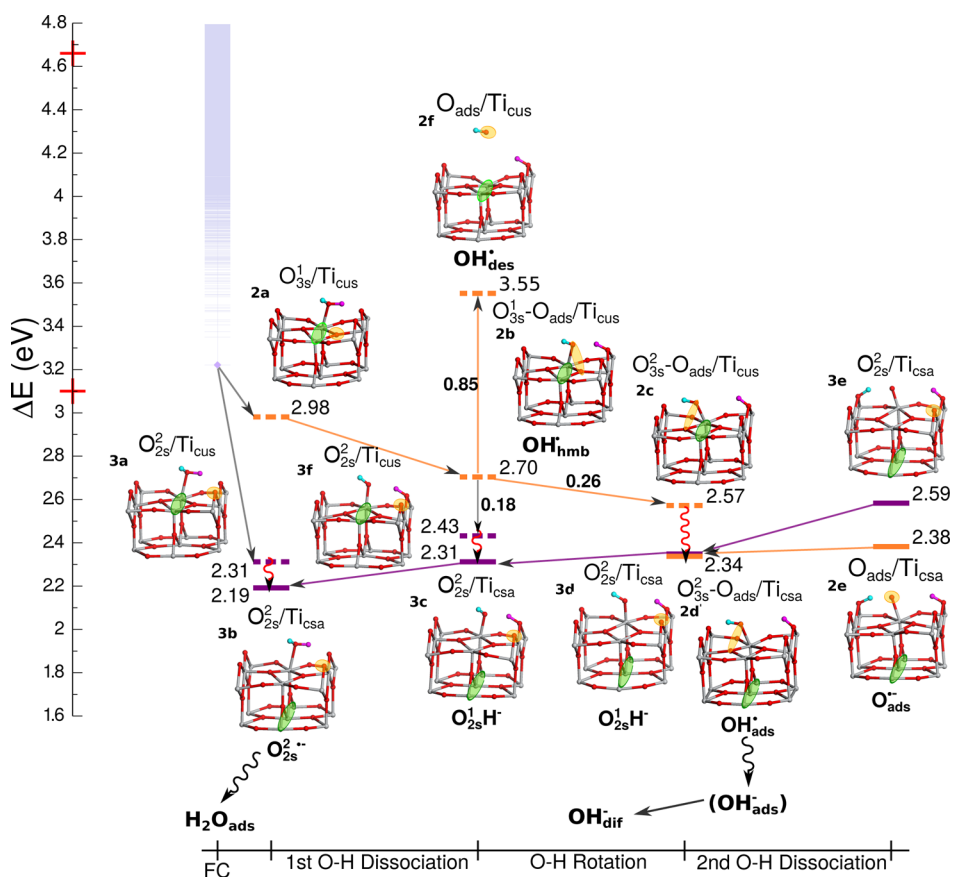
Figure 7. Relationship between the O_{3s}^1 (orange) and O_{2s}^2 (purple) excitons in the photodissociation of H_2O adsorbed at a Ti_{cus} site of $TiO_2(110)$. Green and orange circles denote e and h at Ti and O sites, respectively. Dashed and solid lines denote excitonic configurations where the e resides at the Ti_{cus} and Ti_{csa} sites, respectively. Curly arrows denote nonradiative charge separation via Ti_{cus} to Ti_{csa} e migration (red) and charge-recombination processes (black). Gray arrows connect states with different excitonic character. Red plus signs on the *y*-axis denote experimental excitation energies of ~3.10 and ~4.66 eV, while indigo horizontal lines at the Franck–Condon (FC) point represent vertical excitation energies above the lowest one of ~3.22 eV (tilted square). Formation of $OH_{des}^\bullet$ is only possible in experiments employing 266 nm excitation wavelengths.

electronic configuration. At structure 2f, the hydroxyl group is ~4.15 Å away from the Ti_{cus} site, which represents the desorption limit ~0.85 eV above the 2b minimum.

Both geometric and electronic factors indicate that structure 2f has charge-separated character, with the h located on the hydroxyl group and the e at the farthest Ti_{cus} site. The other electronic configuration that intervenes in the state crossing corresponds to a negatively charged desorbed hydroxyl group, OH_{des}^-, and a protonated substrate with strong Coulomb interaction (~5 eV) and correlates with the structure 1b closed-shell configuration.

The ~3.55 eV desorption limit indicates that the H_2O_{ads} to $OH_{des}^\bullet$ path is only possible for excitation wavelengths ≤~349 nm. This is consistent with the observation of photoinduced H_2O_{ads} oxidation to $OH_{des}^\bullet$ by the 266 nm irradiation wavelength reported in ref 22. The low experimental desorption yields are also consistent with the fact that the path from structure 2b to structure 2c has a lower barrier than the desorption. However, desorption is favored by its irreversibility. In contrast, formation of the desorbed hydroxyl anion OH_{des}^- is disfavored energetically.

3.3. Reactivity of the O_{2s}^2 Exciton. The reactivity of the O_{2s}^2 exciton is shown in Figure 6. The path starts from the excited-state reactant minimum with the O_{2s}^2/Ti_{cus} electronic configuration, 3a, with an energy of ~2.31 eV. The energy separation to the ground state with closed-shell configuration

(dashed gray profile) is only ~0.24 eV. This small energy difference further supports the assignment of the photoluminescence spectra to an analogue of the O_{3s}^1 exciton rather than of the O_{2s}^2 exciton, as suggested in ref 13.

Figure 6 shows that e migration from the Ti_{cus} site to the Ti_{csa} site is exothermic by ~0.12 eV. In contrast, the O−H dissociation from structure 3a (see Figure S2, Supporting Information) is endothermic by ~0.11 eV. Therefore, the most favored path from structure 3a is e migration leading to species 3b, which is the most stable reactant minimum with open-shell electronic configuration (Figures 3 and S2). Importantly, e migration converts the excited-state open-shell 3a species into the ground-state open-shell 3b species through a state crossing. The presence of the crossing and the steepness of the path leading back to H_2O_{ads} suggest that charge carrier recombination to form H_2O_{ads} in this region is highly probable, as indicated by the arrow in Figure 6.

The alternative to charge carrier recombination is to continue along the first O−H bond dissociation coordinate leading to the 3c minimum. For this electronic configuration, the reaction is slightly endothermic by ~0.12 eV and has a barrier of ~0.18 eV.

From structure 3c, the reaction path for the second O−H dissociation proceeds similarly to that described for the O_{3s}^1 exciton, i.e., O−H rotation to bring the second H atom close to the other O_{2s}^1 acceptor, leading to structure 3d, and the H

transfer that leads to the adsorbed formal oxyl dianion 3e. The barrier for O−H rotation is lower than for the O_{3s}^1 exciton (∼0.14 eV vs ∼0.26 eV) because there is no hemibond between the rotating O−H group and the O_{3s} atoms. However, the transfer of the second hydrogen is endothermic by ∼0.48 eV, which indicates that there is no driving force for the dissociation on the O_{2s}^2/Ti_{csa} electronic state.

Figure 6 shows that the proximity to the closed-shell configuration is kept along the entire path. Given that the overall reaction coordinate is endothermic, nonradiative decay from structure 3b to the ground state is more likely to take place than O−H dissociation. This process involves the redistribution of ∼2.7 eV. Charge carrier recombination takes place at the O_{2s}^2 site away from H_2O_{ads}, which implies that the released energy is not redistributed to H_2O_{ads} vibrational modes but to substrate phonons involving the O_{2s}^2 and Ti_{csa} or Ti_{cus} atoms. As a result, water diffusion should not be observed, and ultimately, the 1a reactant should be regenerated. This contrasts what happens in the nonradiative decay of species 2d′ (Figure 5a), which leads to hydroxyl anion diffusion.

The O−H dissociation on the O_{2s}^2 excitonic state may also be relevant in an aqueous medium. At minima 3c and 3d, besides the characteristic stretching of the O−Ti bonds of the O_{2s}^2 atom that carries the h (∼2.0 Å), one of the O−Ti bonds of the O_{2s}^1 atom that carries the H is stretched to ∼2.3 Å (see the inset in Figure 6 and Table S2, Supporting Information). Thus, the presence of a h and a proton on neighboring O_{2s} sites activates the O−Ti bond. This is an important feature because O_{2s}−Ti cleavage is proposed in the nucleophilic attack[14−16] and redox photooxidation[13] mechanisms of OER on rutile TiO_2 in water. The O−Ti stretch introduces partial unsaturation character on the Ti atom, which suggests that, in water, it may undergo a nucleophilic attack, similar to the mechanism postulated previously.[14−16] Alternatively, localization of a second h may induce the cleavage of the Ti−O bond and lead to a species similar to the intermediate reported in ref 54 for water photooxidation on anatase $TiO_2(101)$ (cf. Figure 3A in ref 54), which features an adsorbed hydroxyl radical and a bridging O radical. The two radicals are bound to the same Ti atom and couple to yield a "side-on" η^2-peroxo O−O bond. In this last case, one oxygen comes from adsorbed water and the other one from the surface, whereas, in our case, both oxygen atoms come from the surface. This is consistent with the formation of peroxo species reported in O isotope-labeling experiment studies where both O atoms come from the TiO_2 lattice.[15]

3.4. Reactivity of Other Excitons. The reactivity of other excitons with the h localized on the O_{2s}^1 and O_{ss} sites is shown in Figure S2, Supporting Information. The reactant minima have energies of 2.4−2.6 eV, intermediate between those of the O_{2s}^2 and O_{3s}^1 minima. For the species with the h localized on the O_{2s}^1 atom, we have not located any O−H dissociation path because we have not found any product configuration correlated with the reactant. In turn, the O−H dissociation paths for the O_{ss} exciton configurations are endothermic by ∼0.3 eV. These results suggest that these minima will decay to the most stable O_{2s}^2 exciton or undergo charge recombination, as shown in Figure 2.

4. DISCUSSION

Our discussion is centered on understanding the factors that control the photocatalytic oxidation of H_2O_{ads} on rutile $TiO_2(110)$. These are, primarily, the exciton configuration and the excitation wavelength. We also highlight the role of the

OH species found in the different paths, which are the key players in the photocatalytic activity. Figure 7 shows the reaction paths for the O_{3s}^1 and O_{2s}^2 excitons that explain the formation of different types of radicals and the competition between the paths.

Our calculations indicate that H_2O_{ads} oxidation to the adsorbed hydroxyl radical and oxyl radical anion, $OH_{ads}^\bullet$ and $O_{ads}^{\bullet-}$, is energetically possible with band gap energy excitation. It involves a surface-localized exciton with the h residing at a triply coordinated surface O atom and the e at a nearby surface Ti site (O_{3s}^1 exciton, dashed orange line). However, the path is reversible under UHV conditions, which implies that the net result is no oxidation.

Band gap excitation promotes the formation of a bulk exciton (represented by a tilted square at the Franck−Condon point in Figure 7). The bulk exciton in turn may relax into the O_{3s}^1 localized exciton, which interacts with the water molecule adsorbed nearby, causing the interfacial dissociation of the O−H bond and the simultaneous partial h transfer (PCET mechanism), and leading to the formation of an adsorbed hemibonded hydroxyl radical, $OH_{hmb}^\bullet$. The PCET mechanism explains why the path generating $OH_{hmb}^\bullet$ is barrierless: the localization of the h onto the adsorbate is stabilized by the dissociation of the proton.[63,66] $OH_{hmb}^\bullet$ in turn can evolve into the $OH_{ads}^\bullet$ and $O_{ads}^{\bullet-}$ species. The formation of $OH_{ads}^\bullet$ is exothermic by ∼0.94 eV and is thermodynamically possible with band gap excitation because the h is photogenerated within the $TiO_2(110)$ substrate and subsequently transferred to H_2O_{ads} through the early O_{3s}^1 excitonic intermediate with intact H_2O_{ads} (i.e., indirect mechanism).

In a previous theoretical study, a direct mechanism was proposed where a surface free h is transferred to H_2O_{ads}.[58] The h was found to localize at the O_{3s}^1 site as soon as the H_2O_{ads} had reached the dissociated state. An important difference in comparison with this study is our identification of the early O_{3s}^1 excitonic minimum with intact H_2O_{ads}.

Kinetically, the O_{3s}^1 exciton path features a reaction barrier of ∼0.26 eV associated with hemibond breaking after the PCET. Although the barrier is surmountable with band gap excitation energies, it nevertheless limits the efficiency as it favors the relaxation through a competitive reaction path with a lower energy barrier (∼0.18 eV in Figure 7 and Figure S3, Supporting Information). This path converts the O_{3s}^1 exciton into a surface-localized exciton, with the h residing at a doubly coordinated surface O atom and the e at a nearby surface Ti site (O_{2s}^2 exciton, dashed purple line, discussed below). The fraction of molecules that do not relax to the O_{2s}^2 manifold can react further to $OH_{ads}^\bullet$ and $O_{ads}^{\bullet-}$. However, these are transient, high-energy (∼2.34 and ∼2.38 eV, respectively) species that are prone to undergo charge recombination to diffused hydroxyl anion species, OH_{dif}^-, which implies that the net result is no oxidation. The diffusion of the hydroxyl anion is rationalized by a charge recombination process that takes place at the O atom of the adsorbate. As a result, the released energy is redistributed to the interfacial vibrational modes or adsorbate internal modes that activate the adsorbate's diffusion on the surface. Photo-induced dissociation of H_2O_{ads} leading to an excited-state adsorbed hydroxyl anion OH_{ads}^- species has been reported in a theoretical dynamics study.[79] The process takes place in an excited state associated with Ti defects at interstitial sites of the $TiO_2(110)$ substrate, which is induced at ∼1 eV excitation energies. Although the simulation temperature is consistent with that employed in experiments,[20] no diffusion of the OH_{ads}

species after the dissociation was observed during the simulation. This finding is consistent with the idea that diffusion after O−H bond dissociation is triggered by the vibrational excitation of specific interfacial modes.

To summarize, the formation of $OH_{ads}^{\bullet}$ after band gap excitation is thermodynamically possible but is disfavored by three factors as shown in Figure 7: first, the competition between localization of the initial bulk exciton at the O_{3s}^1 and O_{2s}^1 sites, second, the existence of a competing relaxation channel from the $OH_{hmb}^{\bullet}$ precursor to the lower lying O_{2s}^1 channel, and, third, the propensity of the species to undergo charge recombination and subsequent OH^- diffusion. This explains why $OH_{ads}^{\bullet}$ is not detected experimentally under these conditions.[20,22] However, desorption of the hydroxyl radical from the $OH_{hmb}^{\bullet}$ intermediate is possible at high excitation energies above the desorption limit of ~3.55 eV. The generated free hydroxyl radical, $OH_{des}^{\bullet}$, originates from the adsorbed water molecule, and the desorption process will be favored by direct generation of the h at VB occupied levels with contribution from the H_2O_{ads} $1b_1$ orbital. This can be induced by supra band gap excitation such as the 266 nm wavelength used in some experiments.[22,80] This type of excitation corresponds to an interfacial exciton and is likely to generate $OH_{hmb}^{\bullet}$ after O−H dissociation.

The interfacial exciton mechanism is also consistent with experiments on the photocatalytic activity of rutile nanoparticles in water,[6] where desorption of free hydroxyl radicals is not observed after irradiation with wavelength >300 nm. While this energy exceeds our calculated dissociation limit, it is not sufficient to generate interfacial excitons directly, which suggests that these excitons are necessary to generate the free hydroxyl radicals. In contrast, free hydroxyl radicals are observed for anatase nanoparticles at the same wavelength. Our interpretation is that this may be due to the fact that in anatase the occupied levels with contribution from the water $1b_1$ orbital lie closer to the VBM than in rutile,[29,34] which implies that the interfacial exciton can be generated at longer wavelengths. Moreover, in these levels the weight on water is higher in anatase $TiO_2(101)$ than in rutile $TiO_2(110)$.[29,34] These differences may also influence the desorption barrier to form $OH_{des}^{\bullet}$, and suggest that it should be lower for anatase as compared to rutile. Thus, the formation of free hydroxyl radicals in anatase but not in rutile nanoparticles may also be due to a lower desorption limit for anatase. These considerations are also consistent with the higher efficiency of formation of $OH_{des}^{\bullet}$ observed under UHV with 266 nm excitation for anatase $TiO_2(101)$ as compared to rutile $TiO_2(110)$.[80]

A similar PCET mechanism has been proposed recently for the formation of free hydroxyl radicals in water employing small cluster models and excited-state methods.[43,81] In this mechanism, a free $OH^{\bullet}$ originates from a water molecule of the solvent that is interacting with but not chemisorbed at the surface. While this mechanism appears plausible in water, it should not be the one which explains the scanning tunneling microscopy experiments under UHV conditions of ref 20, as in these experiments the water molecule undergoing oxidation is directly adsorbed on the surface.

The second reaction channel is associated with the O_{2s}^2 exciton, which can be formed from the photogenerated bulk exciton or from nonradiative decay, both to the detriment of the O_{3s}^1 exciton. This exciton is the most representative one at near band gap excitation, since it is the lowest one in energy.

The main cause of the poor photocatalytic activity in UHV at these wavelengths is the high probability of charge recombination along the O_{2s}^2 path. This is due to the near degeneracy between the ground and excited states, which was also observed in a study of photocatalytic water oxidation on small TiO_2 clusters.[81]

While our calculations target UHV experiments, they are also relevant for the experiments in an aqueous medium, as suggested by our assignment of the photoluminescence emitted from atomically smooth (100) and (110) surfaces of rutile TiO_2 in an aqueous medium[14−16] to an excitonic species with the h trapped at an O_{3s} atom (green arrow in Figure 2). Moreover, they indicate that luminescence is not compatible, as suggested in some works,[13] with a species with the h trapped at an O_{2s} atom because the energy separation between the excited and ground energy surfaces is far too small in comparison with the photoluminescence wavelength.

The observed photoluminescence in an aqueous medium suggests that the barrier for PCET from structure 2a will be higher in this medium. The calculations show that h localization at O_{3s}^1 is helped by the incipient formation of a hemibond with an intact water adsorbed at a nearby Ti_{cus} atom, which leans onto the surface to facilitate this interaction (see the distances in Table S1, Supporting Information). This stabilization is probably larger in an aqueous medium where other water molecules from the solvent also contribute, which should result in a higher O−H bond dissociation barrier and higher photoluminescence probability. This would explain why photoluminescence is observed in an aqueous medium, whereas under UHV conditions O−H bond dissociation is favored.

Our results are also consistent with the observed pH dependence of the photoluminescence spectra, whose intensity decreases stepwise with increasing solution pH.[14−16] The solution pH should influence the efficiency of both O_{2s} and O_{3s} decay channels, which compete with the photoluminescence from the O_{3s} excitonic minimum. In an acidic aqueous medium, both the interfacial O−H bond dissociation on the O_{3s} excitonic state and conversion of the O_{3s} exciton into the O_{2s} exciton will be blocked as a consequence of the protonation of the O_{2s} atoms, which would result in efficient photoluminescence. Localization of a h at a protonated O_{2s} atom is predicted to have a positive trapping energy,[53] which makes it unlikely. In contrast, in a less acidic aqueous medium, both processes would take place to the detriment of photoluminescence. The photoluminescence intensity decreases further to almost 0 at pH 13.[14−16] This decrease has been attributed to the oxidation of the oxyl dianion species adsorbed at Ti_{cus} sites (structure 1d in Figure 1) that should form from the dissociation of both H atoms of adsorbed water at this pH. While we cannot rule out this process, our results offer an alternative explanation. They show that the formation of the O_{3s} excitonic minimum is aided by an intact water molecule adsorbed at the Ti_{cus} site. This minimum would hardly form at such a high pH, because the species at the Ti_{cus} site would correspond to a hydroxyl anion rather than an intact water molecule. Thus, the photoluminescence intensity, which is proportional to the density of the O_{3s} excitonic minimum, is sharply decreased at pH 13 due to the dissociation of the water adsorbate on the ground state prior to irradiation. Although the early excitonic O_{3s} minimum with intact H_2O_{ads} would not form, photooxidation of OH_{ads}^- can still take place, but it would be initiated by photoexcitation of OH_{ads}^-, and would proceed with a mechanism similar to that previously observed

for the photooxidation of dissociated absorbed methanol on $TiO_2(110)$.[30,82]

Our results also support the suggestion from the nucleophilic attack mechanism that the surface h trapped initially at an O_{3s} atom, which survives radiative decay, evolves into an O_{2s}-trapped h.[14−16] This is consistent with our calculations because the O_{2s}^2 excitonic state is lower in energy than the O_{3s}^1 excitonic state. Nevertheless, the O_{2s}^2 exciton can also be formed directly after photoexcitation.

Finally, our results support the key role of O_{2s}^2 atoms in OER. While the O_{2s}^2 channel is inactive in UHV because of the high charge recombination probability, this probability will decrease in an aqueous medium due to the stabilization of the charge-separated minima 3b−3d by the polar solvent. Under these conditions, minima 3c and 3d, which have one activated O_{2s}− Ti bond, may be involved in the OER, as explained in section 3.3. This may contribute to explaining the higher photocatalytic activity of rutile in an aqueous medium compared to UHV.

5. CONCLUSIONS

The photocatalytic oxidation of water adsorbed on TiO_2 is one of the most important photocatalytic processes, and our study provides three main new insights.

First, we present a comprehensive picture of the reactivity of water on rutile $TiO_2(110)$ in UHV, a widely used model system.[11,83−85] Our mechanistic picture shows that different hydroxyl species can be formed along competing channels depending on the excitation energy and the nature of the populated exciton. The thermodynamically most stable O_{2s}^2 exciton leads to charge recombination, which explains the overall low reactivity. In turn, the reactive O_{3s}^1 exciton leads, under band gap excitation or above, to the formation of diffused OH_{dif}^- anions after PCET and charge recombination. The formation of the free $OH_{des}^\bullet$ radical, which is the actual oxidation product, is only favored at supra band gap excitation, where it competes with the other channels. In different experiments employing a 266 nm wavelength, both $OH_{des}^\bullet$[22] and HO_{diff}^-[20] have been reported. The amount of $OH_{des}^\bullet$ is an indicator of the amount of H_2O_{ads} that is oxidized as a result of photoinduced OH bond dissociation, whereas the amount of HO_{dif}^- is an indicator of the amount of H_2O_{ads} that is not oxidized even though it has undergone photoinduced OH bond dissociation.

Second, beyond the UHV model system, our results are consistent with a large body of work in an aqueous medium[6,13−16] and provide new insights into the reaction in this medium. Photoluminescence has been used to monitor the OER catalytic efficiency,[14−16] and our computations allow us to assign the O_{3s} exciton as the responsible species. On the basis of our results, we also suggest that the main photocatalytic channel in an aqueous medium corresponds to the O_{2s} exciton. In UHV, this channel is inefficient due to charge recombination, but in an aqueous medium, the charge recombination will be suppressed because of the stabilization of the photocatalytic, charge-separated state by the polar environment. We also propose that one of the photocatalytic paths in an aqueous medium may involve a species with an activated O_{2s}−Ti bond formed from this channel.

Finally, from a more general perspective, and considering our recent study on the photocatalytic oxidation of methanol on rutile $TiO_2(110)$ under the same conditions,[30] our results highlight the fundamental role of excitons in photocatalytic processes and show that fundamental insights into the reaction mechanism and its efficiency can be obtained by treating the excitonic character explicitly in the calculations.

■ ASSOCIATED CONTENT

⑤ Supporting Information

The Supporting Information is available free of charge on the ACS Publications website at DOI: 10.1021/jacs.7b05121.

Total energies and atomic coordinates of all structures, computational details for BSE calculations and validation of the supercell model, Bader and structural analysis, ground-state path for the adsorbed water, H_2O_{ads}, to adsorbed oxo dianion, O_{ads}^{2-}, reaction, first O−H bond dissociation paths of various h−e pairs, and reaction path connecting the O_{3s}^1 and O_{2s}^2 excitons (PDF)

■ AUTHOR INFORMATION

Corresponding Authors
*annapaola.migani@gmail.com
*lluis.blancafort@udg.edu

ORCID ⓘ
Annapaola Migani: 0000-0001-5422-805X
Lluís Blancafort: 0000-0002-0003-5540

Notes
The authors declare no competing financial interest.

■ REFERENCES

(1) Li, X.; Yu, J.; Low, J.; Fang, Y.; Xiao, J.; Chen, X. *J. Mater. Chem. A* **2015**, *3*, 2485−2534.
(2) Ma, Y.; Wang, X.; Jia, Y.; Chen, X.; Han, H.; Li, C. *Chem. Rev.* **2014**, *114*, 9987−10043.
(3) Henderson, M. A. *Surf. Sci. Rep.* **2011**, *66*, 185−297.
(4) Fujishima, A.; Honda, K. *Nature* **1972**, *238*, 37−38.
(5) Fujishima, A.; Zhang, X.; Tryk, D. A. *Surf. Sci. Rep.* **2008**, *63*, 515−582.
(6) Kim, W.; Tachikawa, T.; Moon, G.-h.; Majima, T.; Choi, W. *Angew. Chem., Int. Ed.* **2014**, *53*, 14036−14041.
(7) Diebold, U. *Surf. Sci. Rep.* **2003**, *48*, 53−229.
(8) Jaeger, C. D.; Bard, A. J. *J. Phys. Chem.* **1979**, *83*, 3146−3152.
(9) Kurtz, R. L.; Stock-Bauer, R.; Madey, T. E.; Román, E.; De Segovia, J. L. *Surf. Sci.* **1989**, *218*, 178−200.
(10) Krischok, S.; Höfft, O.; Günster, J.; Stultz, J.; Goodman, D.; Kempter, V. *Surf. Sci.* **2001**, *495*, 8−18.
(11) Brookes, I. M.; Muryn, C. A.; Thornton, G. *Phys. Rev. Lett.* **2001**, *87*, 266103.
(12) Salvador, P. *J. Phys. Chem. C* **2007**, *111*, 17038−17043.
(13) Salvador, P. *Prog. Surf. Sci.* **2011**, *86*, 41−58.
(14) Imanishi, A.; Okamura, T.; Ohashi, N.; Nakamura, R.; Nakato, Y. *J. Am. Chem. Soc.* **2007**, *129*, 11569−11578.
(15) Nakamura, R.; Nakato, Y. *J. Am. Chem. Soc.* **2004**, *126*, 1290−1298.
(16) Imanishi, A.; Fukui, K.-i. *J. Phys. Chem. Lett.* **2014**, *5*, 2108−2117.
(17) Montoya, J. F.; Ivanova, I.; Dillert, R.; Bahnemann, D. W.; Salvador, P.; Peral, J. *J. Phys. Chem. Lett.* **2013**, *4*, 1415−1422.
(18) Montoya, J. F.; Bahnemann, D. W.; Peral, J.; Salvador, P. *ChemPhysChem* **2014**, *15*, 2311−2320.

(19) Micic, O. I.; Zhang, Y.; Cromack, K. R.; Trifunac, A. D.; Thurnauer, M. C. *J. Phys. Chem.* **1993**, *97*, 7277−7283.

(20) Tan, S.; Feng, H.; Ji, Y.; Wang, Y.; Zhao, J.; Zhao, A.; Wang, B.; Luo, Y.; Yang, J.; Hou, J. G. *J. Am. Chem. Soc.* **2012**, *134*, 9978−9985.

(21) Guo, Q.; Xu, C.; Ren, Z.; Yang, W.; Ma, Z.; Dai, D.; Fan, H.; Minton, T. K.; Yang, X. *J. Am. Chem. Soc.* **2012**, *134*, 13366−13373.

(22) Yang, W.; Wei, D.; Jin, X.; Xu, C.; Geng, Z.; Guo, Q.; Ma, Z.; Dai, D.; Fan, H.; Yang, X. *J. Phys. Chem. Lett.* **2016**, *7*, 603−608.

(23) Valdés, A.; Qu, Z.-W.; Kroes, G.-J.; Rossmeisl, J.; Nørskov, J. K. *J. Phys. Chem. C* **2008**, *112*, 9872−9879.

(24) García-Mota, M.; Vojvodic, A.; Metiu, H.; Man, I. C.; Su, H.-Y.; Rossmeisl, J.; Nørskov, J. K. *ChemCatChem* **2011**, *3*, 1607−1611.

(25) Chen, J.; Li, Y.-F.; Sit, P.; Selloni, A. *J. Am. Chem. Soc.* **2013**, *135*, 18774−18777.

(26) Stecher, T.; Reuter, K.; Oberhofer, H. *Phys. Rev. Lett.* **2016**, *117*, 276001.

(27) Krukau, A. V.; Vydrov, O. A.; Izmaylov, A. F.; Scuseria, G. E. *J. Chem. Phys.* **2006**, *125*, 224106.

(28) Heyd, J.; Scuseria, G. E.; Ernzerhof, M. *J. Chem. Phys.* **2003**, *118*, 8207.

(29) Migani, A.; Mowbray, D. J.; Zhao, J.; Petek, H. *J. Chem. Theory Comput.* **2015**, *11*, 239−251.

(30) Migani, A.; Blancafort, L. *J. Am. Chem. Soc.* **2016**, *138*, 16165−16173.

(31) Burdett, J. K.; Hughbanks, T.; Miller, G. J.; Richardson, J. W.; Smith, J. V. *J. Am. Chem. Soc.* **1987**, *109*, 3639−3646.

(32) Kresse, G.; Joubert, D. *Phys. Rev. B: Condens. Matter Mater. Phys.* **1999**, *59*, 1758.

(33) Migani, A.; Mowbray, D. J.; Zhao, J.; Petek, H.; Rubio, A. *J. Chem. Theory Comput.* **2014**, *10*, 2103−2114.

(34) Sun, H.; Mowbray, D. J.; Migani, A.; Zhao, J.; Petek, H.; Rubio, A. *ACS Catal.* **2015**, *5*, 4242−4254.

(35) Migani, A.; Mowbray, D. J.; Iacomino, A.; Zhao, J.; Petek, H.; Rubio, A. *J. Am. Chem. Soc.* **2013**, *135*, 11429−11432.

(36) Mowbray, D. J.; Migani, A. *J. Phys. Chem. C* **2015**, *119*, 19634−19641.

(37) Mowbray, D. J.; Migani, A. *J. Phys. Chem. C* **2016**, *120*, 4151−4151.

(38) Mowbray, D. J.; Migani, A. *J. Chem. Theory Comput.* **2016**, *12*, 2843−2852.

(39) Sheppard, D.; Xiao, P.; Chemelewski, W.; Johnson, D. D.; Henkelman, G. *J. Chem. Phys.* **2012**, *136*, 074103.

(40) Curtarolo, S.; Setyawan, W.; Hart, G. L.; Jahnatek, M.; Chepulskii, R. V.; Taylor, R. H.; Wang, S.; Xue, J.; Yang, K.; Levy, O.; Mehl, M. J.; Stokes, H. T.; Demchenko, D. O.; Morgan, D. *Comput. Mater. Sci.* **2012**, *58*, 218−226.

(41) Salpeter, E. E.; Bethe, H. A. *Phys. Rev.* **1951**, *84*, 1232−1242.

(42) van Setten, M. J.; Gremaud, R.; Brocks, G.; Dam, B.; Kresse, G.; de Wijs, G. A. *Phys. Rev. B: Condens. Matter Mater. Phys.* **2011**, *83*, 035422.

(43) Kazaryan, A.; van Santen, R.; Baerends, E. J. *Phys. Chem. Chem. Phys.* **2015**, *17*, 20308−20321.

(44) Kang, W.; Hybertsen, M. S. *Phys. Rev. B: Condens. Matter Mater. Phys.* **2010**, *82*, 085203.

(45) Baldini, E.; Chiodo, L.; Dominguez, A.; Palummo, M.; Moser, S.; Yazdi-Rizi, M.; Auböck, G.; Mallett, B.; Berger, H.; Magrez, A.; Bernhard, C.; Grioni, M.; Rubio, A.; Chergui, M. *Nat. Commun.* **2017**, *8*, 13.

(46) Liu, L.-M.; Zhang, C.; Thornton, G.; Michaelides, A. *Phys. Rev. B: Condens. Matter Mater. Phys.* **2010**, *82*, 161415.

(47) Migani, A.; Olivucci, M. In *Conical Intersections: Electronic Structure, Dynamics Spectroscopy*; Domcke, W., Yarkony, D. R., Köppel, H., Eds.; Advanced Series in Physical Chemistry, Vol. *15*; World Scientific: Singapore, 2004; pp 271−320.

(48) Migani, A.; Leyva, V.; Feixas, F.; Schmierer, T.; Gilch, P.; Corral, I.; Gonzalez, L.; Blancafort, L. *Chem. Commun.* **2011**, *47*, 6383−6385.

(49) Migani, A.; Blancafort, L.; Robb, M. A.; DeBellis, A. D. *J. Am. Chem. Soc.* **2008**, *130*, 6932−6933.

(50) Migani, A.; Bearpark, M. J.; Olivucci, M.; Robb, M. A. *J. Am. Chem. Soc.* **2007**, *129*, 3703−3713.

(51) Di Valentin, C.; Selloni, A. *J. Phys. Chem. Lett.* **2011**, *2*, 2223−2228.

(52) Nunzi, F.; Agrawal, S.; Selloni, A.; De Angelis, F. *J. Chem. Theory Comput.* **2015**, *11*, 635−645.

(53) Wang, D.; Wang, H.; Hu, P. *Phys. Chem. Chem. Phys.* **2015**, *17*, 1549−1555.

(54) Li, Y.-F.; Selloni, A. *ACS Catal.* **2016**, *6*, 4769−4774.

(55) Zhang, J.; Peng, C.; Wang, H.; Hu, P. *ACS Catal.* **2017**, *7*, 2374−2380.

(56) Ji, Y.; Wang, B.; Luo, Y. *J. Phys. Chem. C* **2012**, *116*, 7863−7866.

(57) Di Valentin, C. *J. Phys.: Condens. Matter* **2016**, *28*, 074002.

(58) Ji, Y.; Wang, B.; Luo, Y. *J. Phys. Chem. C* **2014**, *118*, 1027−1034.

(59) Zhao, W.-N.; Liu, Z.-P. *Chem. Sci.* **2014**, *5*, 2256−2264.

(60) Mowbray, D. J.; Martínez, J. I.; Calle-Vallejo, F.; Rossmeisl, J.; Thygesen, K. S.; Jacobsen, K. W.; Nørskov, J. K. *J. Phys. Chem. C* **2011**, *115*, 2244−2252.

(61) Berardo, E.; Zwijnenburg, M. A. *J. Phys. Chem. C* **2015**, *119*, 13384−13393.

(62) Hoffmann, N. *Eur. J. Org. Chem.* **2017**, *2017*, 1982−1992.

(63) Chen, C.; Shi, T.; Chang, W.; Zhao, J. *ChemCatChem* **2015**, *7*, 724−731.

(64) Petek, H.; Zhao, J. *Chem. Rev.* **2010**, *110*, 7082−7099.

(65) Li, B.; Zhao, J.; Onda, K.; Jordan, K. D.; Yang, J.; Petek, H. *Science* **2006**, *311*, 1436−1440.

(66) Ji, Y.; Wang, B.; Luo, Y. *J. Phys. Chem. C* **2014**, *118*, 21457−21462.

(67) Cheng, J.; VandeVondele, J.; Sprik, M. *J. Phys. Chem. C* **2014**, *118*, 5437−5444.

(68) Deskins, N. A.; Dupuis, M. *J. Phys. Chem. C* **2009**, *113*, 346−358.

(69) Herlihy, D. M.; Waegele, M. M.; Chen, X.; Pemmaraju, C. D.; Prendergast, D.; Cuk, T. *Nat. Chem.* **2016**, *8*, 549−555.

(70) Chen, X.; Choing, S. N.; Aschaffenburg, D. J.; Pemmaraju, C. D.; Prendergast, D.; Cuk, T. *J. Am. Chem. Soc.* **2017**, *139*, 1830−1841.

(71) Matthiesen, J.; Hansen, J. O.; Wendt, S.; Lira, E.; Schaub, R.; Lægsgaard, E.; Besenbacher, F.; Hammer, B. *Phys. Rev. Lett.* **2009**, *102*, 226101.

(72) Wei, D.; Jin, X.; Huang, C.; Dai, D.; Ma, Z.; Li, W.-X.; Yang, X. *J. Phys. Chem. C* **2015**, *119*, 17748−17754.

(73) Wang, Z.-q.; Hao, Q.-q.; Zhou, C.-y.; Dai, D.-x.; Yang, X.-m. *Chin. J. Chem. Phys.* **2015**, *28*, 459−464.

(74) Feng, H.; Tan, S.; Tang, H.; Zheng, Q.; Shi, Y.; Cui, X.; Shao, X.; Zhao, A.; Zhao, J.; Wang, B. *J. Phys. Chem. C* **2016**, *120*, 5503−5514.

(75) Xu, C.; Yang, W.; Ren, Z.; Dai, D.; Guo, Q.; Minton, T. K.; Yang, X. *J. Am. Chem. Soc.* **2013**, *135*, 19039−19045.

(76) Yuan, Q.; Wu, Z.; Jin, Y.; Xu, L.; Xiong, F.; Ma, Y.; Huang, W. *J. Am. Chem. Soc.* **2013**, *135*, 5212−5219.

(77) Guo, Q.; Xu, C.; Yang, W.; Ren, Z.; Ma, Z.; Dai, D.; Minton, T. K.; Yang, X. *J. Phys. Chem. C* **2013**, *117*, 5293−5300.

(78) De Lara-Castells, M. P.; Mitrushenkov, A. O.; Roncero, O.; Krause, J. L. *Isr. J. Chem.* **2005**, *45*, 59−76.

(79) Tritsaris, G. A.; Vinichenko, D.; Kolesov, G.; Friend, C. M.; Kaxiras, E. *J. Phys. Chem. C* **2014**, *118*, 27393−27401.

(80) Geng, Z.; Chen, X.; Yang, W.; Guo, Q.; Xu, C.; Dai, D.; Yang, X. *J. Phys. Chem. C* **2016**, *120*, 26807−26813.

(81) Muuronen, M.; Parker, S. M.; Berardo, E.; Le, A.; Zwijnenburg, M. A.; Furche, F. *Chem. Sci.* **2017**, *8*, 2179−2183.

(82) Kolesov, G.; Vinichenko, D.; Tritsaris, G. A.; Friend, C. M.; Kaxiras, E. *J. Phys. Chem. Lett.* **2015**, *6*, 1624−1627.

(83) Onda, K.; Li, B.; Zhao, J.; Jordan, K. D.; Yang, J.; Petek, H. *Science* **2005**, *308*, 1154−1158.

(84) Onda, K.; Li, B.; Petek, H. *Phys. Rev. B: Condens. Matter Mater. Phys.* **2004**, *70*, 045415.

(85) Lee, J.; Sorescu, D. C.; Deng, X.; Jordan, K. D. *J. Phys. Chem. Lett.* **2013**, *4*, 53−57.